Materials Letters 249 (2019) 33–36

Contents lists available at ScienceDirect

Materials Letters

journal homepage: www.elsevier.com/locate/mlblue

Synthesis of rod-shaped Au-Cu intermetallic nanoparticles and SERS detection

Manish Kumar Singh [a,*], Prajwal Chettri [b], Joysurya Basu [a], Ajay Tripathi [b], Bratindranath Mukherjee [a], Archana Tiwari [b], R.K. Mandal [a]

[a] Department of Metallurgical Engineering, Indian Institute of Technology (BHU), Varanasi 221005, Uttar Pradesh, India
[b] Department of Physics, School of Physical Sciences, Sikkim University, Gangtok 737102, Sikkim, India

ARTICLE INFO

Article history:
Received 6 April 2019
Received in revised form 13 April 2019
Accepted 15 April 2019
Available online 16 April 2019

Keywords:
Intermetallic nanoparticles
Nano-beam electron diffraction
SERS
Methylene blue
Phase transformation
Electron microscopy

ABSTRACT

Intermetallic phases in Au-Cu nanoparticles has been synthesized chemically in liquid phase. The heat-treatment of these nanoparticles at 180 °C for 1 h in solution phase led to the formation of Au-Cu alloy nanoparticles with nearly spherical shapes and monodispersed size of ~10 nm. Subsequent heat-treatment at 300 °C for 30 min of these Au-Cu alloy nanoparticles not only revealed structural transformation to intermetallic phases (tetragonal AuCu (tP4) and cubic Cu_3Au (cP4)) but also shape change occurs from spherical to rods having average aspect ratio ~3.0. The structural determination at the particle has been carried out through nano-beam electron diffraction coupled with simulation of electron diffraction patterns and high resolution phase contrast images. These Au–Cu intermetallic nanoparticles exhibit an excellent surface enhanced Raman spectroscopic activity with methylene blue compared to that of Au-Cu alloy nanoparticles.

© 2019 Elsevier B.V. All rights reserved.

1. Introduction

Intermetallic nanocrystals of controllable shape, size and chemistry are important for their applications in catalysis, plasmonics, and Surface Enhanced Raman scattering (SERS) [1–3]. Liquid phase chemical synthesis is the most common strategy to obtain intermetallic nanoparticles of well-defined shapes and chemistry at relatively lower temperatures compared to their bulk counterpart [1,3,4]. To this end, seeded growth has gained a lot of impetus to synthesize intermetallic nanoparticles [4–6]. The Au-Cu intermetallic nanoparticles have been synthesized by several groups and their catalytic properties have been reported to be superior than that of corresponding random alloys [3,6]. Despite numerous reports on synthesis and characterizations of Au-Cu intermetallic NPs, structural investigation at particle level seems to be scarce [5,7]. Moreover, Au-Cu alloy/intermetallic nanoparticles as SERS substrate is lacking in literature. Herein, we report a non-aqueous solution phase method for synthesis of Au-Cu intermetallic nanoparticles comprised of two step heat-treatment. The heat-treatment temperatures are 180 °C and 300 °C respectively for the formation of Au-Cu solid solution (step I) and Au-Cu intermetallic nanoparticles (step II). Nano-beam electron diffraction (NBD) technique has been adopted to reveal the structures at particle level. SERS activity of random alloy and intermetallic nanoparticles have been investigated for methylene blue molecules.

2. Material and methods

2.1. Synthesis of Au-Cu nanoparticles

Two grams (2 g) hexadecylamine (HDA) (Alfa Aesar) and 125 mg cetyltrimethyl ammonium bromide (CTAB)(Alfa Aesar) were melted at 180 °C [8,9]. This mixture was cooled down to 120 °C in an oil bath. The $AuCl_3$ (Sigma Aldrich) (0.1 mmol) was dispersed in ethanol and was added to the above mixture. The solution turned into dark pink immediately indicating the formation of Au nanoparticles. In this, 0.3 mmol of copper (II) acetylacetonate (Sigma Aldrich) dispersed in ethanol was mixed. The temperature of the bath was raised to 180 °C and solution was heated for about 1 h. The aliquot was taken for the microscopic analysis. In the second step, the temperature was further raised to 300 °C and heat treatment was given for 30 min. The samples were investigated extensively through transmission electron microscope (FEI, Tecnai G^2 T20 operating at 200 kV) for their morphology, structures and chemistry. The nano-beam electron diffraction (NBD) technique was employed to probe the structures at single particle level coupled with computed diffraction patterns

* Corresponding author.
E-mail address: manishkr.rs.met12@itbhu.ac.in (M.K. Singh).

https://doi.org/10.1016/j.matlet.2019.04.065
0167-577X/© 2019 Elsevier B.V. All rights reserved.

by JEMS. For investigating the SERS activity of the substrates Renishaw inVia RM2000 Raman spectrometer was used to collect Raman spectra using 785 nm laser, 50X objective, 10 s exposure and 1.5 mW power.

2.2. Preparation of SERS substrates

A 100 μM stock solution of methylene blue (MB) was prepared in ethanol and was further diluted in ethanol to lower the concentration to 1 μM. The 0.3 mL of 1 μM MB was added to Au-Cu nanopowders. The mixture was then re-dispersed using an ultrasonicator and left undisturbed for 24 h. Finally, the mixture was drop cast on Si-substrate and dried using hot air blower prior to the SERS measurements.

3. Results and discussion

Nearly spherical and monodispersed NPs of average size ~10 nm was observed at 180 °C for 1 h (Fig. 1a and c). Magnified image revealed faceted morphology of the NPs (inset Fig. 1a). Polycrystalline rings was indexed based on FCC with average lattice parameter of ~3.89 Å (Fig. 1b). The reduction in d-values compared to standard FCC-Au and absence of Cu reflections indicates the formation of a single phase solid solution of Cu in Au. The average elemental composition based on STEM-EDS results, of Au and Cu in the Au-Cu nanoparticles was found to be ~66 atom % and ~34 atom % respectively (Fig. 1d). The lattice parameter derived from Vegard's law for this composition was ~3.92 Å. This conforms to observed lattice parameter within experimental error. The TEM and STEM-EDS results therefore establishes formation of Au-Cu alloy.

The representative TEM image with aspect ratio (length/width) as inset and corresponding SAD pattern of Au-Cu nanoparticles processed at 300 °C for 30 min are presented in Fig. 2(a) and (b) respectively. Fig. 2(c) shows high resolution phase contrast image from a rod shaped particle along with FFT (top left) and magnified image (bottom right) as insets. The Au and Cu elemental maps and line scans of a rod shaped particle obtained by HAADF-STEM-EDS are shown in Fig. 2(d)–(i) respectively. Statistics on shape suggests that ~85% of particles change their shape from spherical to rod with average aspect ratio of ~3.0 and remaining to polyhedral shapes with average size of ~80 nm. The polycrystalline diffraction pattern in Fig. 2(b) shows additional rings along with those observed in Fig. 1(b). These extra reflections {1 0 0}, {1 1 0}, {2 1 0} correspond to ordered cubic $AuCu_3$ ($a = 3.75$Å) (cP4) phase (ICDD card no. 035-1357). The fringe spacing of ~0.36 nm and ~0.26 nm corresponding to {1 0 0} and {1 1 0} planes of intermetallic $AuCu_3$ phase substantiates that rods are intermetallic in nature. The average chemistry was found to be ~50 atom % both for Au as well as Cu. The composition of Cu therefore, has increased substantially from 34 atom % to 50 atom % owing to heat treatment at 300 °C for 30 min. The unreacted Cu precursor (at 180 °C for 1 h) seems to have reduced along with promoting diffusion of reduced Cu atoms into already present Au-Cu alloy nanoparticles. The Au and Cu maps of particles as well as line scan across one of rod depict uniform distribution of Au and Cu within the particle (cf.

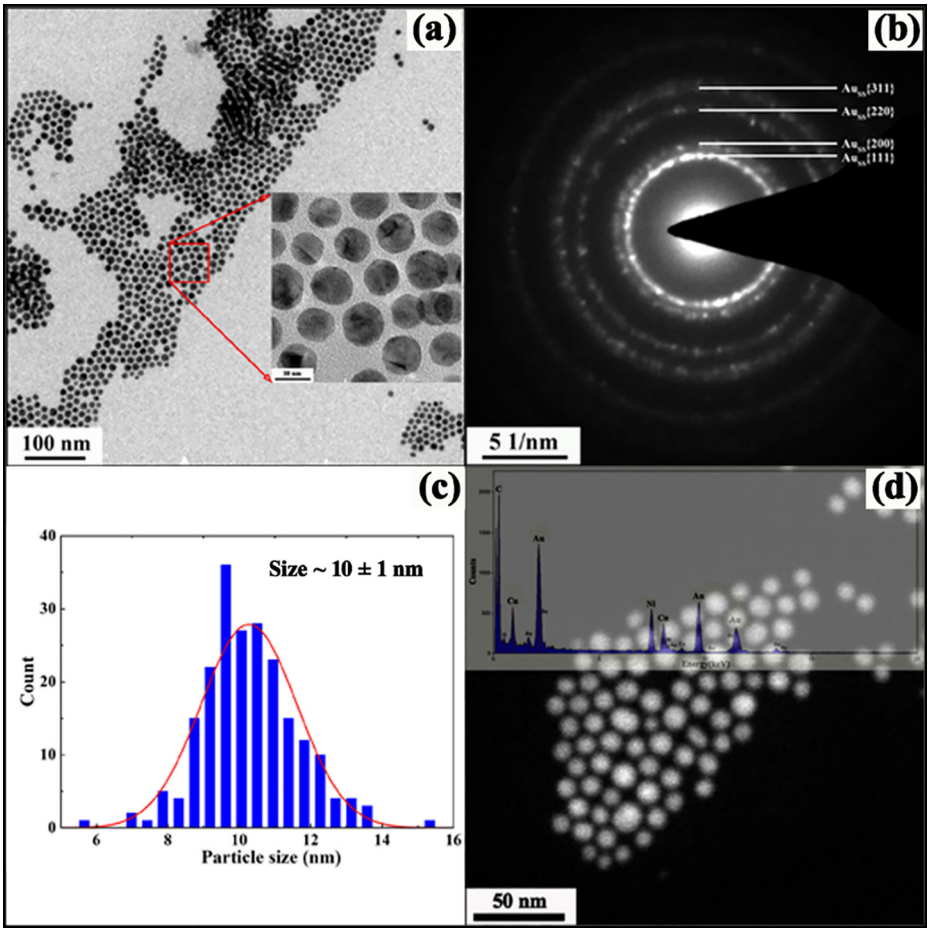

Fig. 1. (a) TEM image with high magnification as inset, (b) corresponding SAD pattern, (c) size distribution histogram, and (d) STEM-EDS of Au-Cu alloy nanoparticles synthesized at 180 °C for 1 h.

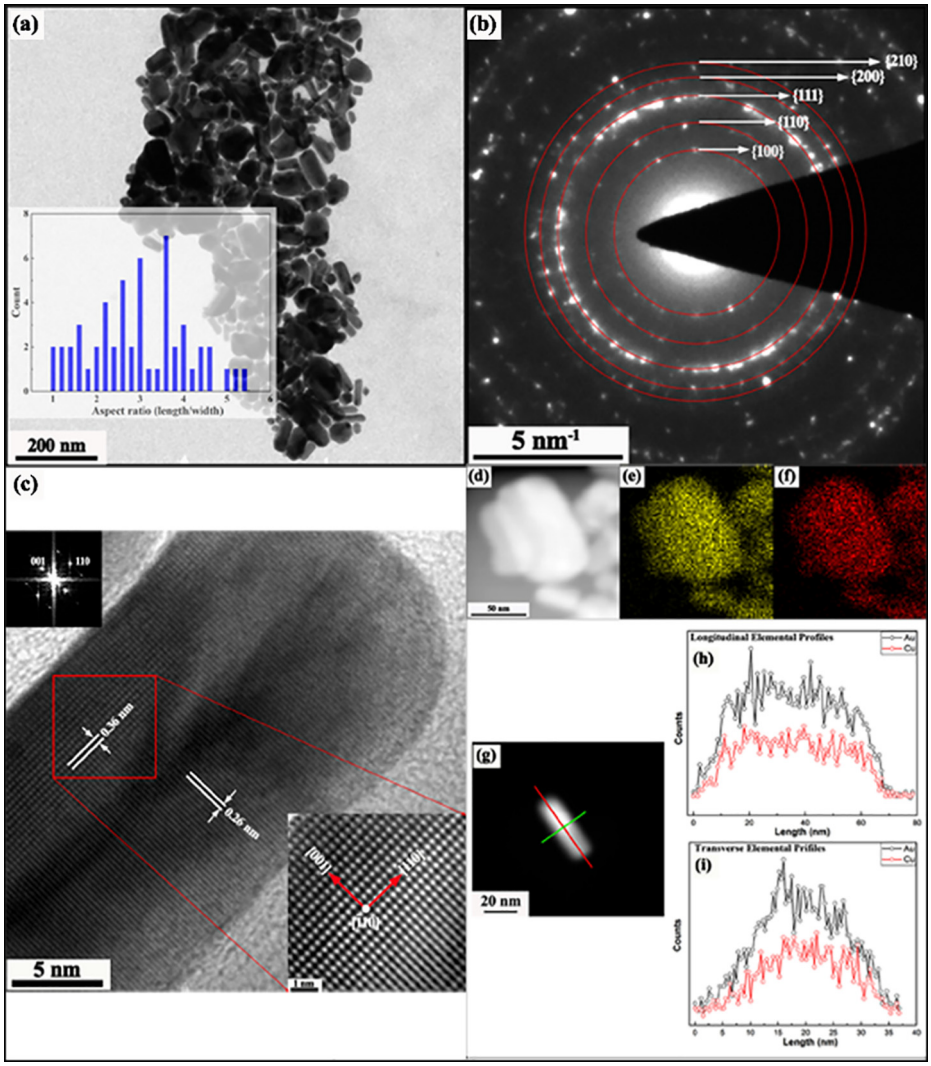

Fig. 2. (a) TEM image with length: width aspect ratio as inset, (b) indexed rings corresponding to Au-Cu intermetallic nanoparticles, (c) high resolution phase contrast image of a nanorod, and STEM-EDS elemental maps (d–f) and line scans of particles (g–i) synthesized at 300 °C for 30 min.

Fig. 2(d)). This further substantiates alloying of Au and Cu in the particles. To probe the structure from single particle, NBD patterns acquired from two such particles coupled with computed patterns is shown in Fig. 3. The indexing of NBD shown in Fig. 3(a) and (b) revealed intermetallic tetragonal AuCu (tP4) (ICDD card no. 03–065-2798) and cubic $AuCu_3$ (cP4) phases with lattice parameters of a = 3.96 Å, c = 3.67 Å and 3.75 Å respectively. The computed patterns shown in Fig. 3(c) and (d) substantiated our indexing of experimentally obtained NBD patterns.

Fig. 3e(i) shows Raman spectrum of 100 μM methylene blue (MB) using Si as a standard substrate. The MB peaks appear at 1622 cm^{-1}, 1380 cm^{-1}, 1180 cm^{-1} and 448 cm^{-1} corresponding to ring stretching of C–C, symmetrical stretching of C-N, stretching of C-N and skeletal deformation of C-N-C respectively. The SERS activity of Au-Cu alloy NPs and

Au-Cu intermetallic NPs is investigated using 1 μM MB as shown in Fig. 3e(ii) and e(iii) respectively. It can be seen from Fig. 3e(ii), weak peak appears at 1441 cm^{-1}(asymmetrical stretching of C–N), 1300 cm^{-1} (in-plane ring deformation of C–H) and 448 cm^{-1} suggesting that Au-Cu alloy NPs does not act as a promising SERS substrate. The dormant nature of Au-Cu alloy NPs towards SERS activity may be attributed to particle size and distribution profile as shown in the TEM image (Fig. 1(a)). It is apparent that the particles are nearly spherical and are monodispersed in nature with average size ~10 nm. The SERS activity is possible for systems where the NPs are present as clusters which act as a 'hotspot' for the enhancement of the Raman signal. Additionally, NPs with asymmetric shape is highly desired for SERS as it facilitates amplification of electromagnetic field present in high concentration at the edges and corners of NPs [10,11]. In contrast, Au-Cu intermetallic NPs shows striking SERS activity as evident from the appearance of strong Raman signatures of MB shown in Fig. 3e (iii). As mentioned earlier, Au-Cu intermetallic NPs have ~85% of facetted and or rod like morphology. In addition, they are uniquely distributed in the form of clusters, which allows for Raman signal enhancement via amplification of electromagnetic radiation. The Raman enhancement factor was calculated to quantitatively examine the enhancement ability of Au-Cu intermetallic NPs using Enhancement Factor (EF) = $I_{SERS}C_{NRS}/I_{NRS}C_{SERS,}$ where I_{SERS} and I_{NRS} is the intensity of the peak with and without SERS substrate corresponding to the concentration C_{SERS} and C_{NRS} of MB used, respectively. The enhancement factor is calculated based on the peak located at 448 cm^{-1}, as it is the strongly enhanced peak within the entire energy range and is found to be 1.2 X 10^3. Authors would further like to point out that SERS activity may considerably change by the adsorption of organic surfactant at the interfaces

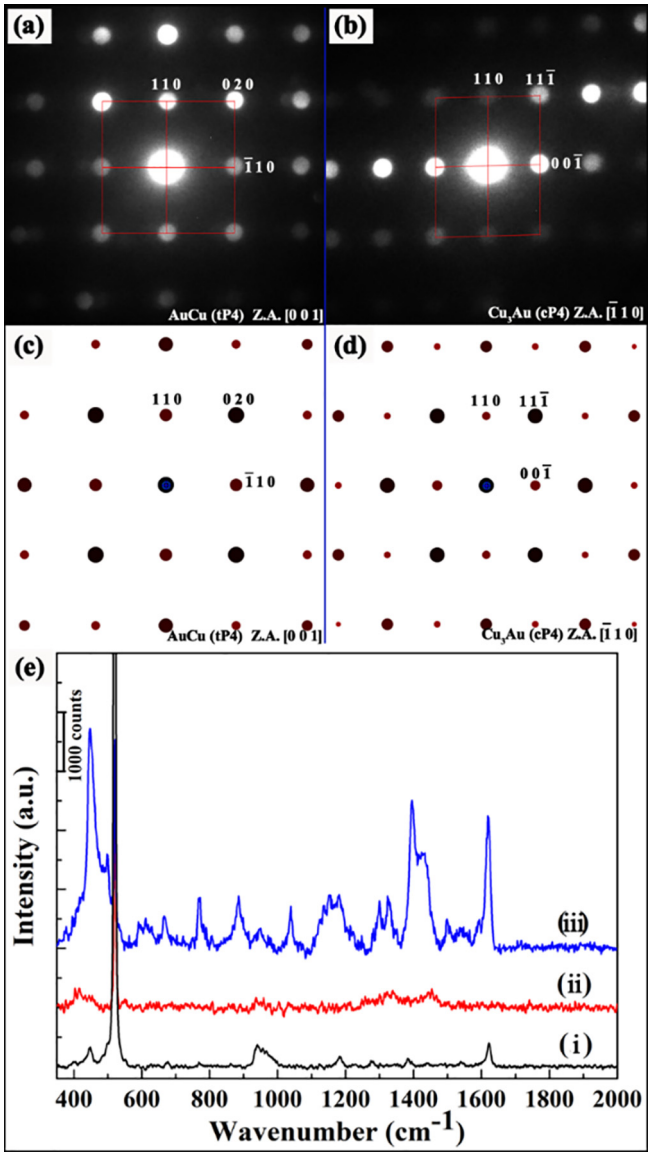

Fig. 3. NBD patterns (a), (b) and corresponding simulated diffraction patterns (c), (d) from two single particles. 3(e) shows Raman spectra (1.5 mW laser power) of 100 μM MB stain on bare Si substrate (i), Raman spectra of 1 μM MB with (ii) Au-Cu alloy, and (iii) Au-Cu intermetallic nanoparticles as a SERS substrate.

between NPs. Adsorption of organic surfactants on particle surfaces and interfaces has been reported earlier by other groups [12,13]. However, the authors would like to argue that the NPs were thoroughly rinsed before SERS experiments in the present work. Additionally, detailed analysis of the TEM results do indicate that the contrast in the NPs is not due to the presence of surfactant at the interface. It is purely due to shape and thickness variation.

In summary, we have reported a facile non-aqueous synthesis of rod-shaped Au-Cu intermetallic nanoparticles of average aspect ratio ~3.0 through solution phase heat-treatment at 300 °C for 30 min. The NBD and simulated DPs revealed tP4 AuCu and cP4 $AuCu_3$ phases at particle level. The rod-shaped Au–Cu intermetallic nanoparticles performed superior SERS enhancement compared to that of nearly spherical Au–Cu alloy nanoparticles of average size ~10 nm.

Conflicts of interest

There are no conflicts to declare.

References

[1] Y. Liu, A.H. Walker, Monodisperse gold-copper bimetallic nanocubes: facile one-step synthesis with controllable size and composition, Angew. Chem. Int. Ed. 49 (2010) 6781–6785.
[2] S. Thota, Y. Wang, J. Zhao, Colloidal Au–Cu alloy nanoparticles: synthesis, optical properties and applications, Mater. Chem. Front. 2 (2018) 1074–1089.
[3] Y. Yan, J.S. Du, K.D. Gilroy, D. Yang, Y. Xia, H. Zhang, Intermetallic nanocrystals: syntheses and catalytic applications, Adv. Mater. 29 (2017) 1605997.
[4] W. Chen, R. Yu, L. Li, A. Wang, Q. Peng, Y. Li, A seed-based diffusion route to monodisperse intermetallic CuAu nanocrystals, Angew. Chem. Int. Ed. 49 (2010) 2917–2921.
[5] M.K. Singh, B. Mukherjee, J. Basu, R. Mandal, Vacancy-mediated structural changes in Au–Cu nanoparticles, Philos. Mag. Lett. 98 (2018) 97–106.
[6] G. Wang, L. Xiao, B. Huang, Z. Ren, X. Tang, L. Zhuang, et al., AuCu intermetallic nanoparticles: surfactant-free synthesis and novel electrochemistry, J. Mater. Chem. 22 (2012) 15769–15774.
[7] R. Mendoza-Cruz, L. Bazan-Diaz, J.J. Velazquez-Salazar, J.E. Samaniego-Benitez, F.M. Ascencio-Aguirre, R. Herrera-Becerra, et al., Order-disorder phase transitions in Au-Cu nanocubes: from nano-thermodynamics to synthesis, Nanoscale 9 (2017) 9267–9274.
[8] T.M. Barnes, M.O. Reese, J.D. Bergeson, B.A. Larsen, J.L. Blackburn, M.C. Beard, et al., Comparing the fundamental physics and device performance of transparent, conductive nanostructured networks with conventional transparent conducting oxides, Adv. Energy Mater. 2 (2012) 353–360.
[9] D. Zhang, R. Wang, M. Wen, D. Weng, X. Cui, J. Sun, et al., Synthesis of ultralong copper nanowires for high-performance transparent electrodes, J. Am. Chem. Soc. 134 (2012) 14283–14286.
[10] R.W. Taylor, R. Esteban, S. Mahajan, R. Coulston, O.A. Scherman, J. Aizpurua, et al., Simple composite dipole model for the optical modes of strongly-coupled plasmonic nanoparticle aggregates, J. Phys. Chem. C 116 (2012) 25044–25051.
[11] S.-Q. Zhu, T. Zhang, X.-L. Guo, X.-Y. Zhang, Self-assembly of large-scale gold nanoparticle arrays and their application in SERS, Nanoscale Res. Lett. 9 (2014) 114.
[12] B. Straumal, A. Mazilkin, S. Protasova, G. Schütz, A. Straumal, B. Baretzky, Observation of pseudopartial grain boundary wetting in the NdFeB-based alloy, J. Mater. Eng. Perform. 25 (2016) 3303–3309.
[13] B.B. Straumal, A. Rodin, A. Shotanov, A.B. Straumal, O.A. Kogtenkova, B. Baretzky, Pseudopartial Grain Boundary Wetting: Key to the Thin Intergranular Layers. Defect and Diffusion Forum, Trans Tech Publ, 2013, pp. 175–192.